J Mater Sci (2014) 49:8107–8115
DOI 10.1007/s10853-014-8518-3

Dielectric nonlinearity and electrical properties of $K_{0.5}Na_{0.5}NbO_3$–$SrTiO_3$ relaxor ferroelectrics

Zhiyong Liu · Huiqing Fan · Changbai Long

Received: 18 June 2014 / Accepted: 28 July 2014 / Published online: 9 August 2014

Abstract $K_{0.5}Na_{0.5}NbO_3$–$xSrTiO_3$($x = 0$, 0.1 and 0.2) ceramics were prepared using the solid-state method. The phase transition behaviors, electrical properties, and electric field-induced dielectric nonlinearity behaviors were investigated as a function of the $SrTiO_3$ content. The electrical properties of the investigated compositions exhibited a significant dependence on the content of $SrTiO_3$. Doped content more than $x = 0.1$ induced a relaxor transformation, while the dielectric loss decreased quickly. In addition, an "extrinsic" polarization contributed to the dielectric nonlinearity behavior of the composition $x = 0.1$ with the polar nanoregions and domain-wall motions, by means of the multipolarization-mechanism model fittings of the electric field dependence of the dielectric permittivity. The dielectric tunability and loss angle tangent of the composition $x = 0.1$ were 32.6 % and 0.028, respectively.

Introduction

In recent years, electric field tunable materials have been extensively used in phase shifters, filters, and microwave devices [1–3], due to high dielectric tunability, low dielectric loss, thermal stability, etc. [4, 5]. Recently, most research efforts mainly focused on ''normal'' ferroelectric materials [6–9]. Also, relaxor ferroelectrics, e.g., $Pb(Mg,Nb,Ti)O_3$ [10], $Ba(Zr,Ti)O_3$ [11], and $Pb_{0.8}Ba_{0.2}ZrO_3$ [12], are potential candidates for electric field tunable materials, which have broad dielectric permittivity peak and strong frequency-dependent behavior. And now, it is commonly recognized that such a broad peak in them is closely related to the response of polar nanoregions (PNRs) [13, 14].

Generally, there are two polarization contributions to the dielectric response of the dielectrics [1, 15, 16]. One comes from "intrinsic" contribution of the lattice phonon polarization, which could be described by the Landau–Ginzburg–Devonshire (LGD) thermodynamic theory. The other stems from the "extrinsic" polarization contributions, such as domain-wall motions, PNRs, and phase-boundary polarization, according to the multipolarization-mechanism model. Compared with the "intrinsic" polarization, the "extrinsic" polarization with different electric fields shows obvious discrepancies, and the corresponding dielectric constant is suppressed more quickly by the external electric field. This indicates that the dielectric tunability could be high owing to the existence of the "extrinsic" polarization. It well explains for the high tunabilities of many ferroelectrics, e.g., $K(Ta,Nb)O_3$ [17], $Ba(Sn,Ti)O_3$ [18], $Pb(Mg,Nb,Ti)O_3$ [11], and $BiFeO_3$ [19].

$K_{0.5}Na_{0.5}NbO_3$ is a compound used as potential piezoelectric and electro-optical applicants due to its excellent piezoelectric, ferroelectric, and electro-optical properties [20–22]. With the $SrTiO_3$ addition, the lead-free $K_{0.5}Na_{0.5}NbO_3$–$SrTiO_3$ solid solutions exhibit proto-typical relaxor ferroelectric behaviors. Correspondingly, their electrostriction effect, electro-optic properties, and electrocaloric effect were well studied [22–25]. However, for realizing applications based on this environmental-friendly system, its electric field dependence of the dielectric permittivity nonlinearity should be investigated. In this work,

Z. Liu · H. Fan (✉) · C. Long
State Key Laboratory of Solidification Processing, School of Materials Science and Engineering, Northwestern Polytechnical University, Xi'an 710072, People's Republic of China
e-mail: hqfan3@163.com

we reported the dielectric nonlinearity and electrical properties of $K_{0.5}Na_{0.5}NbO_3$–$SrTiO_3$ relaxor ferroelectrics, and an increase in the $SrTiO_3$ doping concentration led to a change in phase structures and an improvement in electrical properties. The dielectric nonlinearity of the $K_{0.5}Na_{0.5}NbO_3$–$0.1SrTiO_3$ ceramic was originated from both the "intrinsic" lattice phonon polarization and the "extrinsic" polar nanoregion re-orientations and domain-wall motions.

Experimental details

Ferroelectric polycrystallines $(1-x)$ $(K_{0.5}Na_{0.5})NbO_3$–$xSrTiO_3$ ($x = 0$, 0.1 and 0.2; abbreviated as KNN-xST) were prepared using the solid-state methods. The stoichiometric raw oxides of K_2CO_3, Na_2CO_3, Nb_2O_5, $SrCO_3$, and TiO_2 (Sinopharm Chemical Reagent Co., Ltd, CN) were mixed and then milled using zirconia ball media with ethanol for 12 h. After ball milling, the mixtures were dried and then calcined at 900 °C for 2 h. The precursor powders were ball milled for 24 h again, dried and cold isostatically pressed into pellets with 12 mm in diameter at 300 MPa. The pressed pellets were sintered in the temperature range of 1080–1250 °C for 2 h.

The density of the samples was measured using the Archimedes method. The crystal structures of the samples were detected using X-ray diffraction (XRD) (X'Pert PRO MPD, Philips, Eindhoven, The Netherlands) with CuKα radiation the 2θ range of 20°–60°, and their microstructures were obtained using a field emission scanning electron microscopy (JEOL-6700F, Japan Electron Co., Tokyo, Japan) operated at 20 kV. Raman scattering experiments were performed with an instrument (LabRAM HR800, Horiba JobinYvon, Lyon, France) in a backward scattering geometry (the exciting source was the 514.5-nm line from an argon ion laser).

The sintered pellets were polished to a final thickness of 0.2–0.8 mm, and silver electrodes were coated on both polished surfaces and fired at 550 °C for 30 min for electrical test. Weak-field dielectric responses were measured using a precision impedance analyzer (4294A, Agilent, Santa Clara, CA) associated with a temperature controller (TP94, Linkam, Surrey, U.K.) over a temperature range of 193–773 K at a heating rate of 3 °C/min. The dependence of the ferroelectric polarization (P), current density (J), and the longitudinally field-induced strain (S_{33}) were measured at 10 Hz and 300 K, using a ferroelectric test unit (TF-2000, aix-ACCT, Aachen, Germany). Variable-temperature impedance spectra were performed using an Impedance Analyzer (SI 1260, Solartron, Hampshire, UK). The dc electric field dependence of the dielectric permittivity was measured at 1 kHz and 300 K.

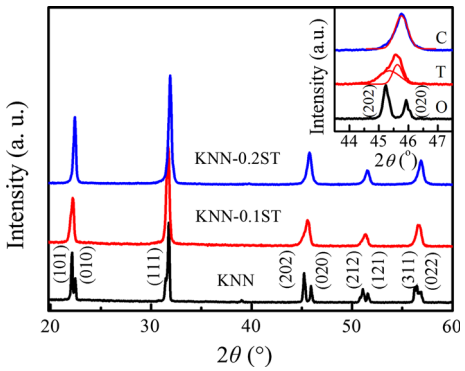

Fig. 1 XRD results of the KNN-xST ceramics in the 2θ range of 20°–60°, the *inset* shows the 2θ range of 43°–47°

Results and discussion

The XRD patterns of the KNN-xST ceramics are shown in Fig. 1, and all the samples have a pure perovskite-phase structure. The pure KNN is orthorhombic phase at room temperature with two natural independent diffraction peaks, (202) and (020), in the $2\theta = 43°$–$47°$ range. Notably, the addition of the ST gives rise to the mergence of the two peaks. For the composition $x = 0.1$, the relatively integrated intensity of the (202) peak is lower than that of the (020) peak with fitting by the Gaussian function. According to Bafandeh et al. and Guo et al. [20, 23], the crystal structure of the KNN-0.1ST sample is tetragonal phase. A further ST addition results in that the (202) and (020) peaks merge a sharp peak with a 2θ angle of 45.8° in KNN-0.2ST sample, indicating that it is cubic phase structure [21]. Additionally, a higher angle shift in diffraction peak is induced by the ST introduced, which is attributed to the shrinkage of the KNN unit cell. The lattice parameters for the KNN-xST ceramics using the software JADE are determined. The lattice parameters of the KNN-0.1ST with a crystal tetragonal symmetry are $a = 3.96137$ Å and $c = 3.97258$ Å, and its tetragonality (c/a) is $= 1.0028$. While the cubic KNN-0.2ST has $a = 3.96436$ Å, very close to that obtained by Kosec et al. [21].

Figure 2 shows the surface and cross-section morphologies of the samples. It is observed that the average grain sizes of KNN-xST ceramics decrease dramatically, accompanying an obvious enhancement in ceramic density. The relative densities of the KNN, KNN-0.1ST and KNN-0.2ST are 90.3, 97.8, and 98.9 %, respectively. The grain size statistical distribution map of KNN-0.1ST sample is demonstrated in Fig. 2d, where the grain size of the sample follows the Gauss distribution (red line) with an average value of 0.37 μm. In addition, a decrease in average grain size is caused with an increase in the content of the ST

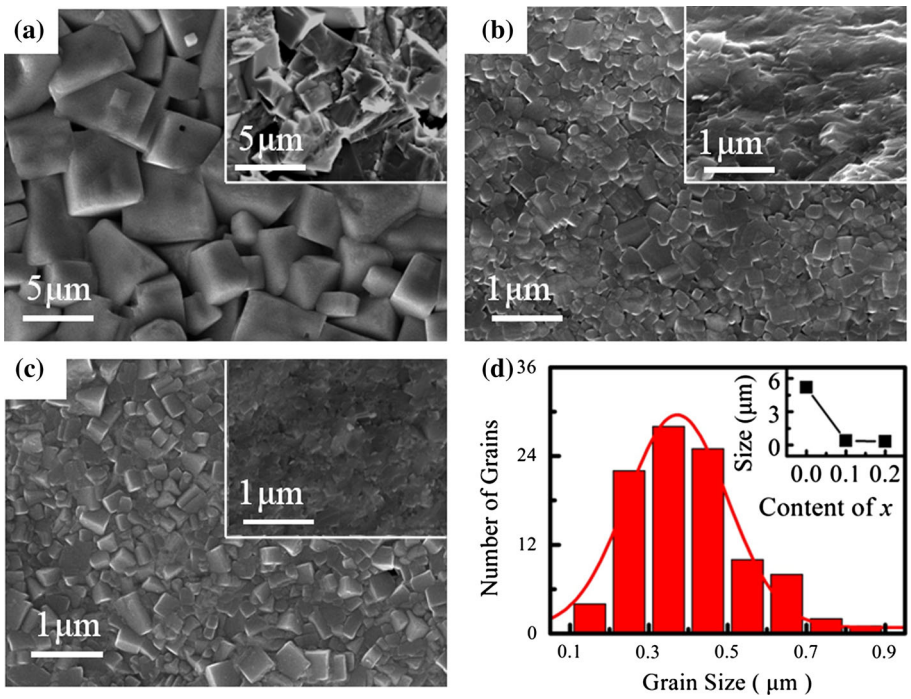

Fig. 2 Surface and cross-section SEM images of the ceramics **a** KNN, **b** KNN-0.1ST, and **c** KNN-0.2ST. **d** Statistical distribution map of grain size of KNN-0.1ST, the inset shows the average grain sizes as a function of ST content

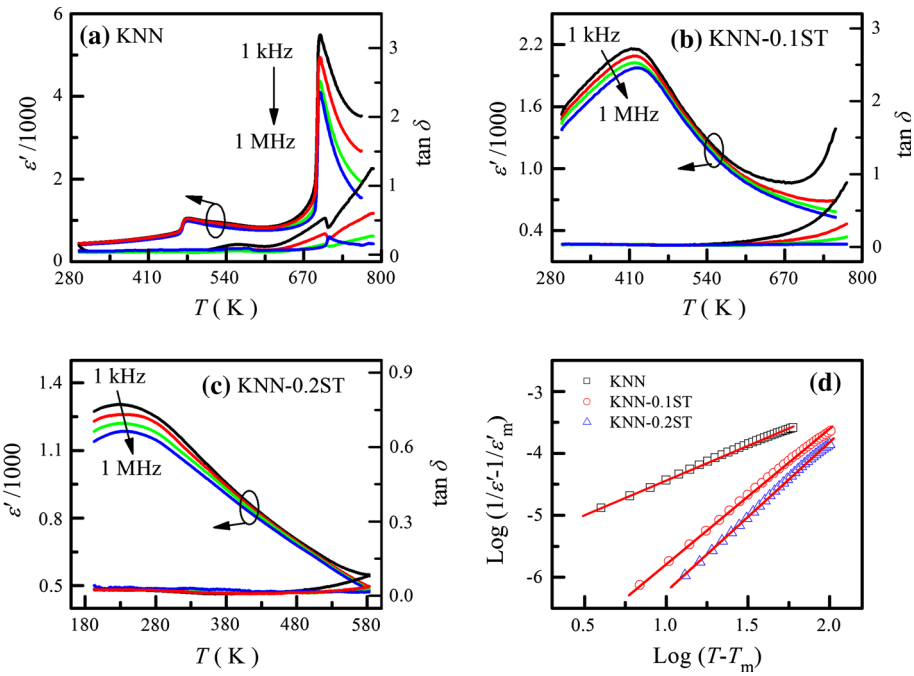

Fig. 3 **a**, **b** and **c** the $\varepsilon'(T)$ and $\tan\delta(T)$ of the KNN-*x*ST ceramics at 1, 10, 100, and 1 MHz, **d** the plots of $\log(1/\varepsilon' - 1/\varepsilon'_m)$ as the function of $\log(T - T_m)$ at 10 kHz of KNN-*x*ST ceramics

addition (inset of Fig. 2d), and the average grain sizes of KNN and KNN-0.2ST are 5.2 and 0.32 μm, respectively.

Figure 3a–c demonstrates the temperature dependences of the dielectric responses and the dielectric loss (tanδ) of the KNN-*x*ST ceramics in the frequency range from 1 kHz to 1 MHz. It is observed that the KNN is a classical ferroelectric with a dielectric sharp peak at 701 K, which is ascribed to the tetragonal to cubic phase transition. With the ST addition, the dielectric peak becomes broadening. Also, the temperatures of the maximum dielectric permittivity (T_m) and the corresponding peak values are decreased as the ST content increases (Table 1). In addition, obvious frequency-dependent behaviors are observed in the ST-modified samples, and the dielectric peaks shift toward higher temperature with the increasing measured frequency. Apparently, the ST-modified samples show

Table 1 The phase transformation temperatures T_m, maximum dielectric permittivity ε'_m, diffusion coefficient γ according modified Curie–Weiss law at 10 kHz

Sample	T_m (K)	ε'_m	γ	t	ε'_{300K}	n_r %	tan δ
KNN	701	5491	1.03	1.018	429	–	0.046
KNN-0.1ST	421	2088	1.97	1.017	1583	32.6	0.028
KNN-0.2ST	232	1259	2.01	1.016	1126	17.4	0.009

The tolerance value t, dielectric permittivity ε'_{300K} at 300 k, tenability (n_r %) and loss (tanδ) of KNN, KNN-0.1ST and KNN-0.2ST ceramics at 1 kHz

obviously diffuse phase transition, which is typical for relaxor ferroelectrics, and their relaxor behaviors are strengthened due to the ST addition increase. For KNN-0.1ST, the T_m varies from 419 to 426 K when frequency is elevated from 1 kHz to 1 MHz, and the corresponding temperature range is 229–237 K for KNN-0.2ST.

For the relaxor ferroelectrics, the reciprocity of the dielectric constant and temperature follows the Uchino and Nomura function, a modified Curie–Weiss law [26],

$$\frac{1}{\varepsilon'} - \frac{1}{\varepsilon'_m} = \frac{(T - T_m)^\gamma}{C}, \quad (1)$$

where C is the Curie constant, and γ is a diffusion coefficient of value ranging from one (a normal ferroelectric) to two (an ideal relaxor ferroelectric). Figure 3d shows the plots of $\log(1/\varepsilon' - 1/\varepsilon'_m)$ as the function of $\log(T - T_m)$ at 10 kHz, where the slope of fitting curves is used to determine the γ values. The γ values of KNN, KNN-0.1ST, and KNN-0.2ST are 1.03, 1.97, and 2.01, respectively. Therefore, it is suggested that an increase in the degree of the relaxor dispersion is accompanied with the increasing ST content.

In general, the origin of the relaxation behavior in ferroelectrics is associated with at least two cations disordering at the same crystallographic site, either A or B. For the present KNN-xST ceramics with the A- and B-site Sr^{2+}/Ti^{4+} co-substitution, their relaxor behaviors could be mainly originated from both A- and B-site cationic disordering. For perovskite with the general formula of ABO_3, the following equation can be used to calculate the tolerance [23]:

$$t = (r_A + r_O)/\sqrt{2}(r_B + r_O), \quad (2)$$

where, r_A, r_B, and r_O are ionics radii of an A-site cation, a B site cation, and an oxygen ion, respectively. The calculation t values are shown in Table 1. Generally, lower t value accompanies lower T_c. It is apparent that the A-site Sr^{2+} (1.44 Å, CN = 12) substitution for Na^+ (1.39 Å, CN = 12) and K^+ (1.64 Å, CN = 12) and the B-site Ti^{4+} (0.605 Å, CN = 6) substitution for Nb^{5+} (0.64 Å, CN = 6) both result in a decrease in t, and lower t is associated with

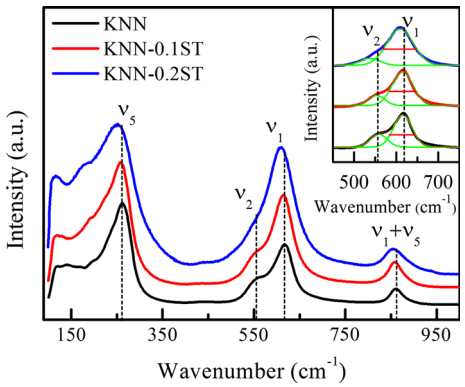

Fig. 4 Raman spectra of KNN-xST ceramics in the wavenumber range from 100 to 1000 cm^{-1}, the inset showing the FWHM of v_1 mode of KNN-xST ceramics

the higher Sr/Ti concentration. Therefore, the ST addition led to a significant decrease in the T_c of the modified KNN-xST ceramics, and consequently the T_c of the composition $x = 0.2$ is observed below room temperature.

The strength of relaxation of KNN-xST ceramics also can be confirmed by Raman spectra. Raman spectra are an appropriate technique to study the dynamics of structure by analyzing the characteristic modes associated to nanoregions in relaxors. By examining the detailed constituent dependence of the characteristic vibrational bands, it is possible to study the dynamics of the nanoregions [23, 27]. Figure 4 demonstrates the Raman spectra of the KNN-xST ceramics in the wavenumber range of 100–1000 cm^{-1}, and there are four intensive modes observed, denoted v_1, v_2, v_5 and $v_1 + v_5$, respectively. The three modes, v_1, v_2, and $v_1 + v_5$, are in response to the NbO_6 octahedron. The mode at <160 cm^{-1} can be assigned to the K^+/Na^+ translational modes due to the similarity to pure alkaline niobates [27]. Inspection from the inset of Fig. 4, an increase in the ST content results in a weak in the v_2 mode, which is similar to the report in other research [23]. In addition, the increasing ST content induces three characteristics: (1) all the Raman modes become broaden; (2) the vibrations mode v_5 due to a coupling of Nb–O symmetry mode, shift to lower frequency; (3) the full width at half maximum (FWHM) of v_1 mode associated with the vibrational modes of the NbO_6 octahedra (The red solid straight lines in the inset of Fig. 4), is increased. The variation of the FWHM of v_1 mode is always used to reveal the dynamic change of the ordered regions [23]. In the present KNN-xST ceramics, the size of the ordered regions and their volume ration to the disordered matrix decreases the ST doping content increases; therefore, the mode v_1 becomes broader. From the above results, probably the co-substitution of Sr^{2+} and Ti^{4+} at the A and B sites of the KNN perovskite structure introduces an increase in the degree of the disorder in the

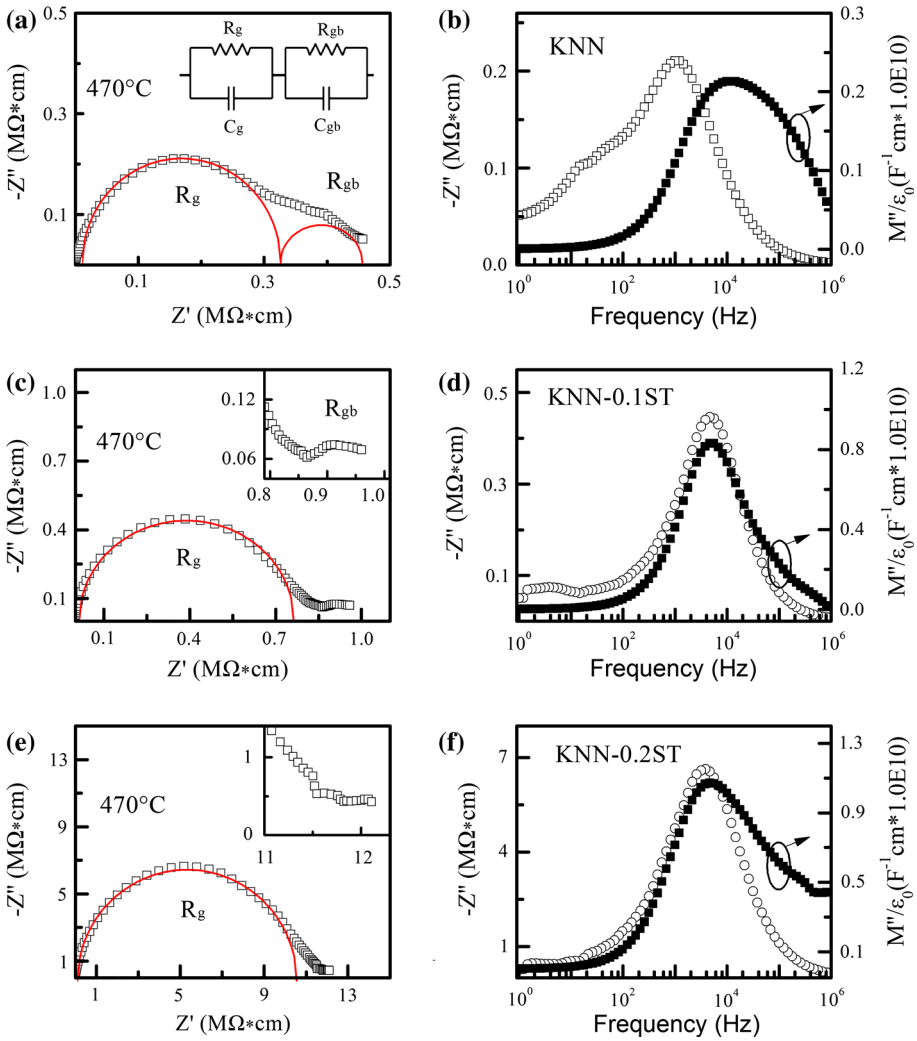

Fig. 5 **a** Impedance complex plane plot and **b** Combined-Z″/M″ spectroscopic plots for KNN, **c** Impedance complex plane plot and **d** Combined -Z″/M″ spectroscopic plots for KNN-0.1ST, **e** Impedance complex plane plot and **f** Combined-Z″/M″ spectroscopic plots for KNN-0.2ST. All samples are measure at 470 °C, frequency range from 1 Hz–1 MHz

structure lattices, giving rise to an enhancement in the relaxation behavior of KNN-*x*ST ceramics. This can be consistent with the results of the modified Curie–Weiss law (Fig. 3d).

Dielectric loss is one of the important factors hindering the dielectric materials to use. Often, there are two types of contributing to the dielectric loss of the ferroelectrics, one is polarization relaxation and the other is electrical conductivity [28]. Although the effect of the polarization is predominant in KNN-*x*ST ceramics, the dielectric loss resulting from the electrical conductivity should be not ignored. Therefore, the impedance spectra (IS) of the KNN-*x*ST ceramics were measured to clarify their electrical conduction behaviors. In Fig. 5a, c and e, the electrical resistivities (ρ) of the samples have a significant dependence on the ST content, and an increase in ρ induced with increasing the ST content. Commonly, IS data can be modeled on an equivalent circuit consisting of three parallel RC elements connected in series, electrode, grain boundary, and grain components, respectively, from low frequency to high frequency. However, only two arcs are observed for KNN at 470 °C (Fig. 5a), where the high-frequency semicircle is attributed to grain effect and the low-frequency semicircle is due to the grain boundary effect. The corresponding plots of the imaginary part of impedance, Z″ (Fig. 5b), also show shoulder peaks associated with the grain boundary and grain effects [29, 30]. By contrast, the ST substitution leads to an improvement in grain effect and a weak grain boundary effect. The complex impedance spectra of the KNN-0.2ST sample (Fig. 5e) are characterized by a single semicircle. The corresponding Z″/M″ spectroscopic plots with the same data (Fig. 5f) almost show a single peak with maxima at high frequency, and the lower frequency peak nearly disappears. This indicates that with the ST content addition increase, the samples become essentially one electrical component and are therefore electrically homogeneous. Hence, the observed macroscopic dielectric loss processes

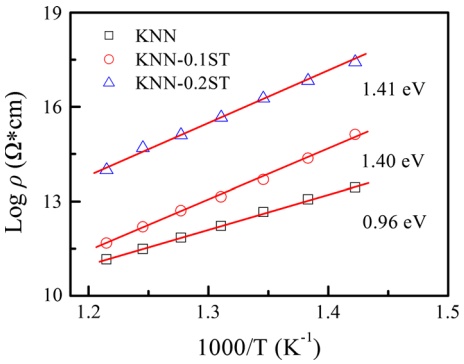

Fig. 6 Arrhenius plots of the grain resistivities of KNN-*x*ST ceramics

are attributed to microscopic conduction and polarization mechanism occurring inside the grain, while grain boundary contributions are negligible.

Furthermore, logarithmic grain resistivities (ρ) of those samples in the temperature range of 430–550 °C are shown in Fig. 6. Correspondingly, the activation energy (E_a) for electrical resistivity can be determined using the Arrhenius equation:

$$\rho = \rho_0 \exp\left(\frac{-E_a}{kT}\right), \tag{3}$$

Where E_a is the nominal activation energy per charge carrier, and k is the Boltzmann constant. The E_a value of the pure KNN is 0.96 eV (see in Fig. 6). Interestingly, the ST modification induces a significant increase in ρ, and the resistivity of the composition $x = 0.2$ at each temperature is increased by one order of magnitude. Also, the activation energy is increased dramatically, and the E_a values of the KNN-0.1ST and KNN-0.2ST ceramics content are upto 1.40 eV. The intrinsic conduction (the band gap) is mainly determined by the NbO_6 octahedron, and the Nb(4d) state at the conduction-band edge has an important influence on the electronic conductivity [31]. Therefore, the low-valence state Ti^{4+} substitution at a Nb^{5+} site could induce a more broad band gap and cause a decrease in intrinsic conductivity, which may lead to an increase in ρ and E_a in the ST-modified samples. As a result, the dielectric losses of the modified KNN-*x*ST samples were decreased obviously.

Figure 7a shows a classic hysteresis loop of normal ferroelectric for pure KNN, and its *J*-*E* loop demonstrates a sharp switching current peak, which indicates the domain reverse under the electric field. Comparatively, KNN-0.1ST sample (Fig. 7b) exhibits a slim but well-defined hysteresis loop, and the switched current peak in the corresponding *J*-*E* loop is found to be obviously suppressed. This may be ascribed to the existence of local nanopolar clusters and a few microdomain in the domain structure. Moreover, the *P*-*E* loop of KNN-0.2ST sample (Fig. 7c) turns slimmer, which is almost a straight line, and no obvious switched current peak is observed in the *J*-*E* loop; it is concluded that the microdomain contribution in KNN-0.2ST are disappearance. In addition, the ST substitution gives rise to a significant decrease in remnant polarization (P_r) as well as the maximum polarization (P_{max}), and the coercive field (E_c) of the modified KNN-*x*ST ceramics also is reduced extraordinarily. Figure 7d shows the bipolar field-induced strains of the KNN-*x*ST ceramics ($x = 0.1$, 0.2). A butterfly-type strain curve is observed for KNN-0.1ST, and the strain value is 0.061 % at 50 kV/cm, with increasing the ST content to $x = 0.2$, the *S*-*E* curve is almost hysteresis-free and the strain value is decreased to be 0.019 %. Since the KNN-0.2ST is in the paraelectric state according to the XRD and dielectric permittivity results, its hysteretic nonlinear behavior should be attributed to a result of field-induced weak ferroelectricity [14].

Although the pure KNN has a strong ferroelectricity, the dc-tunability property is very weak [32]. Figure 8 shows the dc-tunability of the KNN-0.1ST and KNN-0.2ST compositions are determined at 1 kHz and 300 K. An obvious nonlinearity of the $\varepsilon'(E)$ dependence is observed for both compositions. The dielectric tunability (n_r) was calculated using the following expression:

$$n_r = (\varepsilon'(0) - \varepsilon'(\mathrm{E}))/\varepsilon'(0), \tag{4}$$

where $\varepsilon'(0)$ and $\varepsilon'(\mathrm{E})$ represent the dielectric permittivity at zero and under a certain electric field, respectively. It is observed that an increases in the ST-substituted concentration results in a decrease in $n_r(50\mathrm{kV/cm})$, from 32.6 % ($x = 0.1$) to 17.4 % ($x = 0.2$). The dielectric tunability of KNN-0.1ST sample is close to that reported in Ref. [6] ($n_r = 44$ % at 70 kV/cm), and higher to that reported in Ref. [32] ($n_r = 13$ % with an $E = 800$ kV/cm). In the relaxor-ferroelectric materials, not only the polarization mechanism associated with the lattice phonon polarization contribution can be considered, but also the PNRs and the boundaries of microdomains can contribute to the total polarization and tunability.

To further understand this dielectric nonlinear behavior of the KNN-*x*ST ceramics ($x = 0.1$ and 0.2), the LGD thermodynamic theory was applied [1]:

$$\begin{aligned}\varepsilon'(E) &= \varepsilon'(0)/\left\{1 + \lambda\left[\varepsilon_0\varepsilon'(0)^3E^2\right]\right\}^{1/3} \\ &= \varepsilon_1' - \varepsilon_2'E^2 + \varepsilon_3'E^4 + \cdots\end{aligned} \tag{5}$$

where $\varepsilon_1' = \varepsilon'(0), \varepsilon_2' = (1/3)\lambda\varepsilon(0)^4, \varepsilon_3' = (2/9)\lambda^2\varepsilon(0)^7$, etc., ε_0 is vacuum dielectric permittivity, λ is a temperature-independent coefficient, $\varepsilon'(0)$ is the relative dielectric permittivity at zero field, and $\varepsilon(0)$ is the dielectric permittivity at zero field ($\varepsilon(0) = \varepsilon_0\varepsilon'(0)$). The parameter ε_1' is the linear dielectric permittivity, and the parameters $\varepsilon_2', \varepsilon_3'$,

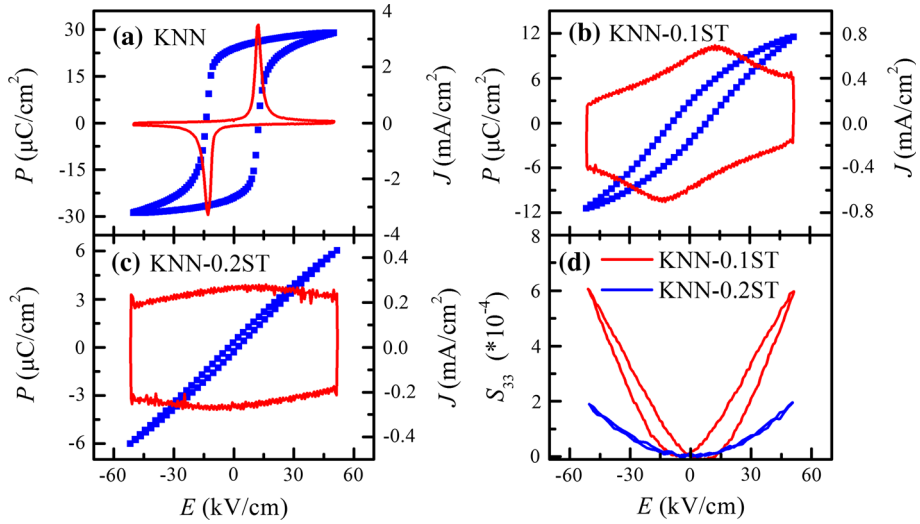

Fig. 7 **a**, **b** and **c** ferroelectric *P*-*E* loops, *J*-*E* loops of KNN-*x*ST ceramics, **d** field-induced strains of KNN-*x*ST ceramics

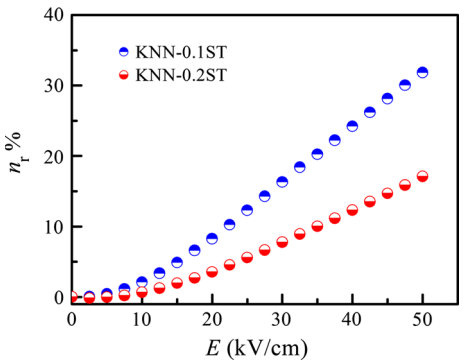

Fig. 8 The tunability (n_r %) of KNN-*x*ST ceramics

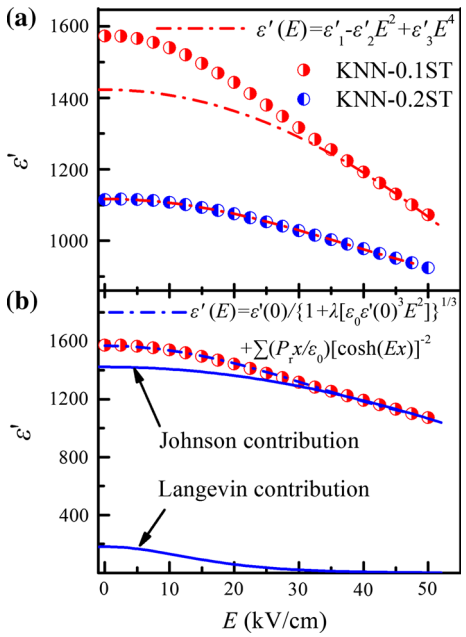

Fig. 9 **a** ε'(E) of KNN-*x*ST ceramics fitting by LGD theory, **b** ε'(E) of KNN-0.1ST ceramic fitting by multipolarization-mechanism model

and higher order terms are the nonlinear dielectric permittivities, respectively. Additionally, all the dielectric parameters are temperature dependent.

It can be seen from Fig. 9a that excellent fitted result of the ε'(E) was observed in the KNN-0.2ST sample. However, the fitting ε'(E) data of the KNN-0.1ST were mismatched, as compared to the experimental data. It is probable that there is more than one polarization contributing to the dielectric response of the KNN-0.1ST. One could come from an intrinsic contribution of the lattice phonon polarization which can be described by the LGD thermodynamic theory, and the other may be related to some "extrinsic" polarization contributions, *e.g.*, PNRs and domain-wall motions. Relatively, the polarization contribution to the $\varepsilon'(E)$ behavior of the KNN-0.2ST sample could be only caused by the lattice phonon polarization, and no "extrinsic" polarization contribution is observed. Taking into account the contribution of the "intrinsic" and "extrinsic" polarizations to the ε'(E) of the KNN-0.1ST, approximations, a multipolarization-mechanism model is suggested in the present work, and the following equation is adopted to describe the field dependence of the dielectric permittivity [15, 16]:

$$\varepsilon'(E) = \varepsilon'(0)/\left\{1+\lambda\left[\varepsilon_0\varepsilon'(0)^3E^2\right]\right\}^{1/3} + \sum(P_r x/\varepsilon_0)[\cosh(Ex)]^{-2}, \quad (6)$$

where the former term represents the lattice polarization induced from the LGD theory, and the latter represents there clusters polarization contribution (Langevin contribution). The P_r is the effective polarization of one cluster,

L is the cluster size k_B is Boltzmann's constant, and $x = P_r L^3/(k_B T)$. $\sum$ is intended as the sum of polarization terms over different "extrinsic" contributions. In this case two terms (PNRs and domain-wall motions) have to be taken into account to correctly describe the dielectric response. The fitting to experimental data in Fig. 9b shows that the proposed multipolarization-mechanism model works, namely, an excellent fit for KNN-0.1ST. In addition, the contribution of the PNRs and domain-wall motions (Langevin contribution) was separated from the overall dielectric response. It can be seen that the sum of PNRs and domain-wall motions terms acts at low fields, while the contribution of the "extrinsic" mechanism to the dielectric constant is around 12 % for KNN-0.1ST sample.

Conclusions

Pure perovskite structure KNN-xST ($x = 0$, 0.1 and 0.2) ceramics were synthesized using the solid-state reaction. Raman spectra indicated the co-substitution of Sr and Ti induced an outstanding cationic disorder in the structure lattices, giving rise to a notable ferroelectric relaxation. The electrical properties of the investigated compositions exhibited a significant dependence on the content of ST addition. With doped increased, the T_c was decreased from 701 to 232 K, and the corresponding electrical resistivity increased significantly. The multipolarization-mechanism model fitting results indicated that the dielectric nonlinearity of the KNN-0.1ST sample was contributed from both the "intrinsic" lattice phonon polarization and the "extrinsic" PNRs and domain-wall motions.

Acknowledgements This work was supported by the National Natural Science Foundation (51172187), the SPDRF (20116102130002, 20116102120016) and 111 Program (B08040) of MOE, and Xi'an Science and Technology Foundation (CX12174, XBCL-1-08), and Shaanxi Province Science Foundation (2013KW12-02), and the NPU Fundamental Research Foundation (NPU-FRF-JC201232) of China.

References

1. Bianchi U, Dec J, Kleemann W, Bednorz JG (1995) Cluster and domain-state dynamics of ferroelectric $Sr_{1-x}Ca_xTiO_3$ ($x = 0.007$). Phys Rev B 51:8737–8746
2. Kong LB, Li S, Zhang TS, Zhai JW, Boey FYC, J Ma (2010) Electrically tunable dielectric materials and strategies to improve their performances. Prog Mater Sci 55:840–893
3. Xu Q, Zhan D, Liu HX, Chen W, Huang DP, Zhang F (2013) Evolution of dielectric properties in $BaZr_xTi_{1-x}O_3$ ceramics: Effect of polar nano-regions. Acta Mater 61:4481–4489
4. Astafiev KF, Sherman VO, Tagantsev AK, Setter N (2003) Can the addition of a dielectric improve the figure of merit of a tunable material? J Eur Ceram Soc 23:2381–2386
5. Chung UC, Elissalde C, Maglione M, Estournès C, Paté M, Gann JP (2008) Low-losses, highly tunable $Ba_{0.6}Sr_{0.4}TiO_3$/MgO composite. Appl Phys Lett 92:042902(1–3)
6. Chen YC (2006) Effect of DC biasing field on dielectric properties of ZrO_2-doped barium strontium titanate. J Mater Sci 41:5836–5840. doi:10.1007/s10853-006-0293-3
7. Jiang H, Zhai J, Zhang M, Yao X (2012) Enhanced microwave dielectric properties of $Ba_{0.40}Sr_{0.60}TiO_3$–$Zr_{0.80}Sn_{0.20}TiO_4$ composite ceramics. J Mater Sci 47:2617–2623. doi:10.1063/1.2364127
8. Sun X, Yang Y, Zhang Q, Zhou X, Hu Z, Huang C (2014) Enhanced dielectric and tunable properties of barium strontium titanate thin films through introducing $Nd(Zn_{1/2}Ti_{1/2})O_3$ and adjusting Ba/Sr. J Mater Sci 49:1058–1065. doi:10.1007/s10853-013-7783-x
9. Ke S, Huang H (2010) Giant low frequency dielectric tunability in high-k $Ba(Fe_{1/2}Nb_{1/2})O_3$ ceramics at room temperature. J Appl Phys 108:064104(1-6)
10. Peng B, Fan H, Zhang Q (2012) The contribution of the "extrinsic" polarizations to the dielectric tunability of $Pb(Mg_{1/3}Nb_{2/3})_{1-x}Ti_xO_3$ relaxor ferroelectrics. J Am Ceram Soc 95:1651–1655
11. Ke S, Fan H, Huang H, Chan HLW, Yu S (2008) Dielectric dispersion behavior of $Ba(Zr_xTi_{1-x})O_3$ solid solutions with a quasiferroelectric state. J Appl Phys 104:034108(1–7)
12. Peng B, Fan H, Zhang Q (2013) High tunability in (111)-oriented relaxor $Pb_{0.8}Ba_{0.2}ZrO_3$ thin film with antiferroelectric and ferroelectric two-phase coexistence. J Am Ceram Soc 96:1852–1856
13. Wei X, Yao X (2006) Analysis on dielectric response of polar nanoregions in paraelectric phase of relaxor ferroelectrics. J Appl Phys 100:064319(1–6)
14. Cross LE (1987) Relaxor ferroelectrics. Ferroelectrics 76:241–267
15. Chen A, Zhi Y (2004) dc electric-field dependence of the dielectric constant in polar dielectrics: multipolarization mechanism model. Phys Rev B 69:174109(1–8)
16. Chen A, Bhalla AS, Cross LE (2001) Dielectric behavior of paraelectric $KTaO_3$, $CaTiO_3$, and $(Ln_{1/2}Na_{1/2})TiO_3$ under a dc electric field. Phys Rev B 64:184104(1–6)
17. Li H, Tian H, Gong D, Meng Q, Zhou Z (2013) High dielectric tunability of $KTa_{0.60}Nb_{0.40}O_3$ single crystal. J Appl Phys 114:054103(1–3)
18. Curecheriu LP, Ianculescu AC, Horchidan N, Stoleriu S, Tudorache F, Tascu S, Mitoseriu L (2011) Temperature dependence of tunability of $Ba(Sn_xTi_{1-x})O_3$ ceramics. J Appl Phys 109:084103(1–5)
19. Curecheriu L, Gheorghiu F, Ianculescu A, Mitoseriu L (2011) Non-linear dielectric properties of $BiFeO_3$ ceramics. Appl Phys Lett 99:172904(1–3)
20. Bafandeh MR, Gharahkhani R, Lee JS (2014) Enhanced electric field induced strain in SrTiO3 modified (K, Na)NbO3-based piezoceramics. J Alloys Compd 602:285–289
21. Kosec M, Bobnar V, Hrovat M, Bernard J, Malic B, Holc J (2004) New lead-free relaxors based on the $K_{0.5}Na_{0.5}NbO_3$–$SrTiO_3$ solid solution. J Mater Res 19:1849–1854
22. Kroupa J, Petzelt J, Malic B, Kosec M (2005) Electro-optic properties of KNN-STO lead-free ceramics. J Phys D Appl Phys 38:679–681
23. Guo Y, Kakimoto K, Ohsato H (2004) Ferroelectric-relaxor behavior of $(Na_{0.5}K_{0.5})NbO_3$-based ceramics. J Phys Chem Sol 65:1831–1835
24. Bobnar V, Malič B, Holc J, Kosec M, Steinhausen R, Beige H (2005) Electrostrictive effect in lead-free relaxor $K_{0.5}Na_{0.5}NbO_3$–$SrTiO_3$ ceramic system. J Appl Phys 98:024113(1–4)
25. Rožič B, Koruza J, Kutnjak Z, Cordoyiannis G, Malič B, Kosec M (2013) The electrocaloric effect in lead-free $K_{0.5}Na_{0.5}NbO_3$–$SrTiO_3$ ceramics. Ferroelectrics 446:39–45

26. Uchino K, Nomura S (1982) Critical exponents of the dielectric constants in diffused-phase-transition crystals. Ferroelectrics Lett 44:55–61
27. Polomaka M, Hilczer B, Kosec M, Malic B (2008) Raman scattering studies of lead free $(1 - x)$ $K_{0.5}Na_{0.5}NbO_3$–$x$$SrTiO_3$ relaxors. Ferroelectrics 369:149–156
28. Jonscher AK (1975) Physical basis of dielectric loss. Nature 253:717–719
29. Li M, Sinclair DC (2012) The extrinsic origins of high permittivity and its temperature and frequency dependence in $Y_{0.5}Ca_{0.5}MnO_3$ and $La_{1.5}Sr_{0.5}NiO_4$ ceramics. J Appl Phys 111: 054106(1–8)
30. Li M, Sinclair DC, West AR (2011) Extrinsic origins of the apparent relaxor like behavior in $CaCu_3Ti_4O_{12}$ ceramics at high temperatures: a cautionary tale. J Appl Phys 109:084106(1–9)
31. Neumann T, Borstel G, Scharfschwerdt C, Neumann M (1992) Electronic structure of $KNbO_3$ and $KTaO_3$. Phys Rev B 46: 10623–10627
32. Abadei S, Gevorgian S, Cho CR, Grishin A, Andreasson J, Lindbäck TDC (2001) Field dependent properties of $Na_{0.5}K_{0.5}NbO_3/SiO_2/Si$ structures at millimeter-wave frequencies. Appl Phys Lett 78:1900–1902